



# Aneurysm segmentation algorithm

## *deliverable – D3.1*

Project acronym: **THROMBUS**,

Project full title: A quantitative model of thrombosis in intracranial aneurysms

- Instrument type: Collaborative Project
- Project coordinator: CNRS

- Contract nr.: FP7-ICT-2009-6- 269966
- Start date: Feb 1, 2011
- Duration: 36 months

### Report identification

Period from: 01/02/2011  
 To: 01/02/2011  
 Due date of report: 01/02/2012 (+45 days)  
 Submission date: 01/03/2012  
 Revision: Final

#### Dissemination level:

PU = Public

**X**

### Partners involved

Authors of this report	<b>Olivier Bernard and Guy Courbebaisse</b>	<b>CNRS - CREATIS</b>	
Contributors involved in the reported work (from same organisation or others)	<b>Jean-Philippe Thiran</b>	<b>EPFL</b>	



## Table of Contents

1	Executive Summary .....	6
2	Introduction .....	6
3	Methods and Results .....	8
3.1	Data base building.....	8
3.1.1	Database used to validate the current segmentation work .....	8
3.1.2	Database in a long time vision .....	9
3.2	Segmentation of both aneurysm and adjacent vessel structures .....	9
3.2.1	Specification .....	9
3.2.2	Strategy .....	11
3.2.3	Evaluation / validation .....	13
3.3	Segmentation of the aneurysm structure.....	17
3.3.1	Specification .....	17
3.3.2	Strategy .....	18
3.3.3	Proposed algorithm : an improved version of subjective surface .....	18
3.3.4	Originality .....	19
3.3.5	Evaluation / validation .....	24
3.4	Segmentation of the lumen and of the thrombus of the aneurysm.....	26
3.4.1	Specification.....	26
3.4.2	Strategy .....	27
3.4.3	Algorithm .....	27
3.4.4	Originality .....	28
3.4.5	Validation.....	28
4	Conclusion .....	29
4.1	Conclusion on the segmentation of both aneurysm and adjacent vessel part .....	29
4.2	Conclusion on the segmentation of the aneurysm alone .....	29
4.3	Conclusion on the segmentation of both the lumen and the thrombus of the aneurysm .....	29
4.4	Work in progress .....	29
5	References.....	30

## List of tables

Table 1: Summary of the parameters settings used for the segmentation of the database. First column: image name. Second column: algorithms used. Third column: Parameters involved. Forth and fifth columns: number of iterations and CPU time needed to reach final results.

Table 2: Time spent to separate the aneurysm from the adjacent vessels. First column: image name. Second column: number of iterations. Third column CPU time needed to reach final results

## List of Figures

Fig. 1: Example of images involved in the database to segment cerebral aneurysm with adjacent vessel structures. a) 3DRA image. b) 3DRA with dose image. c) CTA image.

Fig. 2: Intensity profile of an 3DRA volume

Fig. 3: Intensity profile of a MIP image created from the volume given in Fig. 1-a

Fig. 4: Segmentation results of two 3DRA images using state-of-the-art methods. First line: Gan model. Second line: Chan-Vese model. Third line: Holtman-Grazit model

Fig. 5 a: Segmentation results of two 3DRA with dose images using state-of-the-art methods. First line: Gan model. Second line: Chan-Vese model. Third line: Holtman-Grazit model

Fig. 5 b: Segmentation results of one CTA image using state-of-the-art methods. First line: Gan model. Second line: Chan-Vese model. Third line: Holtman-Grazit model

Fig. 6: Left: Kanizsa triangle. Right: 2D slice of an aneurysm with and adjacent vessel. The red curves are illusory contours

Fig. 7: 2-D example of aneurysm segmentation from a rotational angiography image. (a, from left to right) original data, edge detector, segmented contour, in red, superimposed to original data. (b, from left to right): evolution of the initial point-of-view surface and selection of a level set, red line, for segmentation.

Fig. 8. Illustration of the influence of the level value on the quality of the segmentation of an aneurysm. Segmentation result obtained for a normalized level value equals to (a) 0.3, b) 0.5 and c) 0.7.

Fig. 9. Illustration of the effect of the first term of the evolution equation on the behavior of the subjective surface. In this particular case, the subjective surface only evolves from a  $g$  function equals to 1 everywhere. (a) Initial state. b) Subjective surface after 100 iterations. c) Subjective surface after 200 iterations.

Fig. 10. Segmentation of a 2D slice of an aneurysm from a rotational angiography imaging using subjective surface theory. The red line corresponds to the level at which we extract the contour displayed on the first row.

Fig. 11. 2D illustration of the creation of the initial mask inside the aneurysm

Fig. 12. Initialization procedure applied on a Rotational Angiography image (a) and a Computed Tomography Angiography image (b).

Fig. 13. Aneurysm segmentation results of two 3DRA images using a modified version of the subjective surface algorithm. First column: Vessel segmentation using Holtman-Grazit method. Second column: Aneurysm segmentation result

Fig. 14. Aneurysm segmentation results of a CTA image using a modified version of the subjective surface algorithm. Left image: Vessel segmentation using Holtman-Grazit method. Right image: Aneurysm segmentation result

Fig. 15. Aneurysm segmentation results of two 3DRA images with dose using a modified version of the subjective surface algorithm. First column: Vessel segmentation using Holtman-Grazit method. Second column: Aneurysm segmentation result

Fig. 16. Illustration of the visualization of the 3D contour extracted from the aneurysm segmentation result.

Fig. 17. Angiographic medical image of aneurysm

Fig. 18. Segmentation of the lumen (b) and of the thrombus (f) of the image (a)

## 1 Executive Summary

---

In this deliverable, the progress of the segmentation tasks for aneurysm segmentation is explained. The goal is to describe the status of the development and validation of the methods for aneurysm segmentation in 3D Computed Tomography angiography (CTA), Magnetic Resonance angiography (MRA) and Digital Subtraction Angiography with three-dimensional reconstruction (3DRA).

The segmentation of aneurysm structures has been widely studied in the literature. The goal of this task in the project is to design a complete image processing tool for the extraction of the different aneurysm structures with the following constraints:

- Accurate segmentation of aneurysm and adjacent vessels.
- Near real time algorithm implementations.
- Very limited user interaction for the complete extraction of the structures.
- Compatibility with the global processing pipeline of Thrombus.

The main achievements of the research at its current state can be summarized as follows:

- A first database of 5 images has been created in order to test and validate our algorithms.
- A long time vision database that would provides CTA, MRA and 3DRA images for ten patients before and after endovascular intervention has been initialized with the CHU of Montpellier.
- Three different 3D segmentation algorithms have been implemented to evaluate the difficulty in segmenting vessels in CTA and 3DRA imaging.
- A modified version of subjective surface has been developed for the segmentation of the aneurysm from the adjacent vessels.
- A global strategy has been designed to reduce the user interaction to one simple click to provide the segmentation of both the aneurysm and the adjacent vessels.
- A first attempt for thrombus segmentation has been investigated based on Lattice Boltzmann method.
- A segmentation validation strategy has been initialized with the CHU of Montpellier and with the HCL partners.

## 2 Introduction

---

The goal of this deliverable is to present a progress report on the aneurysm segmentation part. Indeed, we have already design a strategy to automatically segment and separate the aneurysm and adjacent vessels from conventional modalities. In the sequel, we present in detail the work that has been done and present the results we obtain from a database that we start to build via the HCL partner.

Also to better understand the thrombosis phenomena, we have worked on thrombosed aneurysms images with the objective to quantify the thrombus lumen rate, along the treatment of the considered aneurysms. An original method based on the Lattice Boltzmann Method has been implemented to segment both lumen and thrombus of cerebral aneurysms. To date the proposed solution treats 2D cases.

### Vessel and aneurysm sac segmentation

Automatic segmentation in 3D medical images is a difficult task due to noise, inhomogeneous image

gradient, and the presence of vessels of a wide range of sizes. Some of the re initial approaches for 3D vascular segmentation are based on statistical thresholding. These techniques approximate the distribution of probabilities of the intensity values in the image by finite mixture models (FMM) estimated from the expectation maximization algorithm. The FMM allows obtaining segmentation by means of an automatic global thresholding. These methods have been applied to the segmentation of the cerebral vascular tree and cerebral aneurysms in time of flight (TOF) and phase contrast (PC) magnetic resonance angiography (MRA) (*Wilson and Noble, 1999; Chung et al., 2004*), and in 3D rotational angiography (3DRA) (*Gan et al., 2005*).

The most recent approaches for 3D vascular segmentation are based on deformable models. The model is represented by a surface that deforms for recovering the shape of the vascular structure. In vascular analysis, cylindrical or line-like shapes parameterized by the vasculature centerlines are frequently used (*Frangi et al., 1999; Krissian et al., 2000; Yim et al., 2001; de Bruijne et al., 2003; Aylward and Bullitt, 2002; Wink et al., 2004; Fridman et al., 2004; Volkau et al., 2005*). In many cases, these models are not able to extract a complex arterial tree without substantial user interaction. Moreover, the tubular constraint usually prevents the model from representing pathological shapes as stenosis or large aneurysms.

The use of geometric deformable models within the level set framework (*Osher and Sethian, 1988*) has become very popular. Their ability to handle changes of topology and adapt to the shape of complex structures makes them a very suitable technique for the automatic segmentation of complex vascular structures and, more concretely, of cerebral aneurysms.

In geometric deformable models solely based on gradient information (*Geodesic Active Contours, Caselles et al., 1997*), the evolution of the deformable surface strongly depends on the image quality. Due to limited resolution or artefacts present in medical imagery, the gradient usually presents discontinuities at the boundaries and inside narrow locations of the objects. The evolving surface suffers from leakage in such places. Moreover, the curvature and edge constraints prevent the surface to evolve through narrow and twisted vessels. To deal with these limitations, some improvements to this model have been proposed in the literature for the segmentation of vascular structures in MRA, 3DRA and CTA, that consist of smart initializations of the model (*Deschamps, 2001; Antiga et al., 2003; van Bemmelen et al., 2003; Hernandez and Frangi, 2004*), modifications in the energy functional (*Lorigo et al., 2000; Deschamps, 2001; Hernandez and Frangi, 2004; Yan and Kassim, 2006; Manniesing et al., 2006; Holtzman-Gazit et al., 2006*), or hybrid approaches (*Chen and Amini, 2004*).

## Thrombus segmentation

As we have seen, many automated methods for lumen and aneurysm sac segmentation have been reported in the literature. Thrombus segmentation, however, remains a difficult segmentation problem due to the low contrast between thrombus and surrounding tissue in CTA images. Approaches based on image gradient fail because strong responses from neighbouring objects, such as the spine, lumen, and calcifications, distract the method from finding the correct boundary. Threshold-based approaches also fail, since similar image intensity can be found inside the thrombus and in the neighbouring structures. For these reasons, the level of automation and/or accuracy of existing thrombus segmentation methods remain low. Only few methods for thrombus segmentation have appeared in

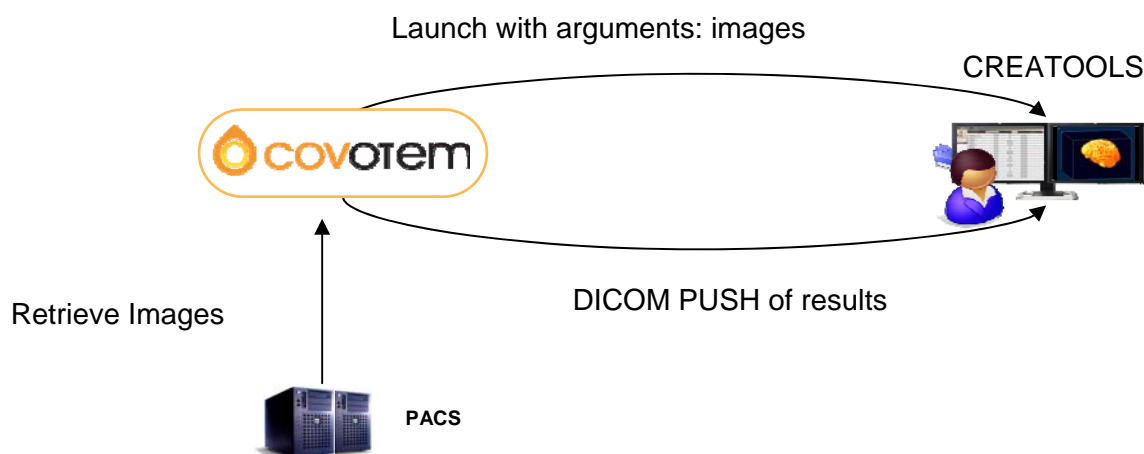
the literature. The method by De Bruijne et al. in ([de Bruijne et al., 2004](#)) is based on active shape models (ASM). The reported results are accurate, but the amount of user intervention is large, since slice-by-slice control is required. The method in ([Subasic et al., 2002](#)) is based on 3D level-sets. Although user intervention is minimal, the reported results are not accurate. Another method proposed in ([de Bruijne et al., 2003](#)) uses a 3D ASM with a grey level appearance model based on a nonparametric pattern classification technique. Reported results are accurate, but the amount of interaction for initialization is still significant. The method proposed in ([Giachetti and G. Zanetti, 2004](#)) segments the thrombus slice-by-slice with a 2D DM initialized with dilated cross-sections of the lumen boundary, which is segmented from a sphere, similarly to ([Subasic et al., 2002](#)). The thrombus is deformed based on a strong shape constraint and an image feature combining intensity gradient and threshold. The amount of user intervention is significant, due to slice-by-slice control, and accuracy is not reported. Recent works have been provided by using the lattice Boltzmann method dedicated to image processing, with the objective to segment regions of the brain ([Chen, 2009](#)) without the need of user interaction.

### 3 Methods and Results

#### 3.1 Data base building

##### 3.1.1 Database used to validate the current segmentation work

The Collaborative system based on COVOTEM and CREATOOLS (Cf D5.2), has been installed between HCL Lyon - Neuroradiology department, COVALIA and CNRS - CREATIS.



The collaborative system allows users to query a PACS (Picture Archiving and Communication System) in order to visualize all DICOM images of a hospital. Users are able to choose one or several DICOM exams and retrieve them on their computer. During this retrieve, anonymisation function is applied and a case file is automatically created.

From this collaborative system, we have collected 5 patient specific aneurysms in different modalities: 2 angiography images (named in the sequel RA1 and RA2), 2 digital subtraction angiography images (named RAS1 and RAS2) and one computed tomography angiography (named CTA1).



### 3.1.2 Database in a long time vision

CNRS in agreement with the consortium will subcontract in 2012, the acquisition of medical imaging sequences with several medical imaging modalities, dedicated to the study of the behavior of Intracranial Aneurysms, by the association Gui de Chauliac. The purpose of this subcontract is to provide relevant data in order:

- to provide systematic medical data for several patient specific aneurysms following the protocol approved by the Medical Ethic committee of the CHU of Lyon (cf D5.1). Neuroradiologists need to fill an observation notebook or CRF (Case Report Form) for each case during one year when stent is implanted in the brain of the patient.
- to study more specifically the wall of the cerebral aneurysms; two objectives are pointed: towards a more realistic modeling of the wall of the aneurysm, and a mean to estimate the mechanical properties of the wall, for the implementation in the numerical simulation code.

## 3.2 Segmentation of both aneurysm and adjacent vessel structures

### 3.2.1 Specification

The following specification part has been strongly inspired by the interesting recent work of [Hernandez and Frangi, 2007](#) and [Holtzman-Gazit et al., 2006](#). A cerebral aneurysm is an abnormal enlargement of any artery located in the brain. This pathology tends to appear at or near bifurcations of the arteries in the Circle of Willis. The purpose of this part is to present a recent state of the art of automatic methods for segmentation of cerebrovascular structures with application to the segmentation of brain aneurysms in 3D Rotational Angiography (3DRA) and Computed Tomography Angiography (CTA). Segmentation in 3DRA is a difficult task due to noise, inhomogeneous image gradient, and the presence of vessels of a wide range of sizes. Fig. 1a and 1b shows some examples of 3DRA images (with and without dose) in these situations. Segmentation in CTA is even more challenging because of the presence of bone tissue in the image with intensity values that highly overlap with vessel tissues. As shown in Fig. 1-c, these images present high partial volume artifacts especially in locations where the vessel is close to or touching other vessels, the aneurysm, or the skull.

Since the method of region competition proposed by Zhu and Yuille (1996), there have been several works that include statistical region-based information in the geometric deformable model ([Paragios, 2000](#); [Yezzi et al., 1999](#); [Chan and Vese, 2001](#); [Aubert et al., 2003](#); [Pichon et al., 2004](#)). In these different versions of geodesic active regions (GAR), the surface is deformed according to an evolution equation that minimizes an energy functional depending not only on the gradient but also on region-based statistical information. In places with weak gradients, region-based information drives the evolution of the surface thus avoiding non-desirable effects of gradient-driven evolution. Some of these versions even completely drop gradient information. Thus, the segmentation accuracy fully relies on region-based information ([Chan and Vese, 2001](#); [Pichon et al., 2004](#)). The GAR model includes region-based statistical information defined in terms of the probability associated with a region  $R$ .

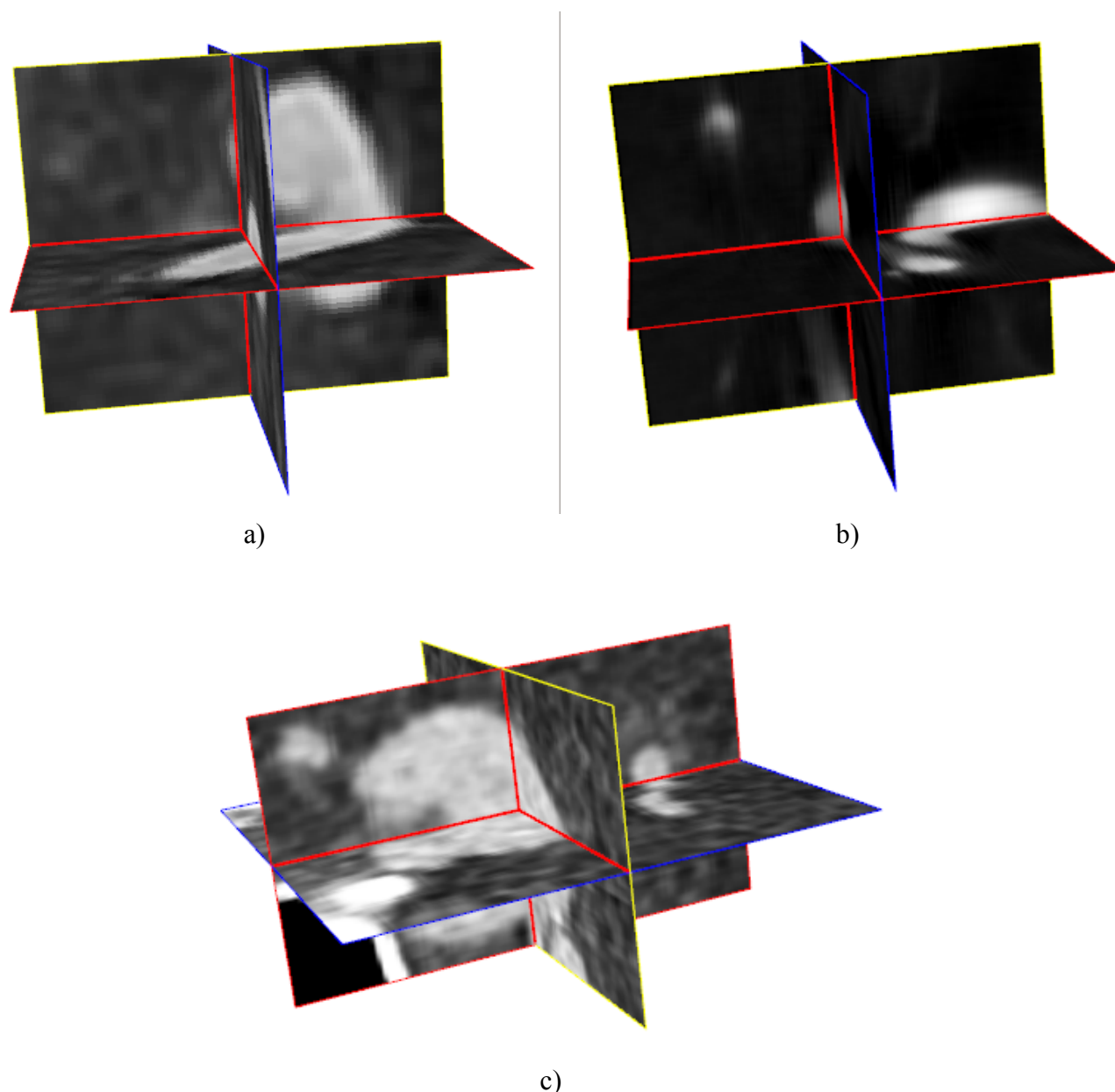


Fig. 1: Example of images involved in the database to segment cerebral aneurysm with adjacent vessel structures. a) 3DRA image. b) 3DRA with dose image. c) CTA image.

### Region-based geometric deformable models

In the case of medical images, each region is assumed to be in correspondence with a tissue. The estimation of the probabilities for each tissue involves the definition of the feature space that characterizes the image inside the different tissues. In most previous attempts, the estimation of the probabilities is based on two main assumptions: image intensity is the most discriminant tissue descriptor and the statistics of the intensity distribution can be described using parametric estimators. In particular, the probabilities are usually modeled with a finite mixture model ([Zhu and Yuille, 1996](#); [Paragios, 2000](#)) or even simpler assumptions ([Yezzi et al., 1999](#); [Chan and Vese, 2001](#); [Aubert et al., 2003](#)). More recently, [Hernandez and Frangi, 2007](#) designed a region descriptor that incorporates high-order multiscale features in a non-parametric statistical framework. The underlying feature space is derived from a training dataset.

### 3.2.2 Strategy

From the previous state-of-the-art, we decided to focus our interest on region-based geometric deformable models and more particularly on level-set since these methods appear to give very interesting results. In this context, we propose to study models involving features computed directly from the image itself and without any learning stage strategy as in [Hernandez and Frangi, 2007](#). Indeed, we believe that features derived from training dataset are too much dependent on the involved data and so on the equipment used to create the dataset. In the sequel, after a brief presentation of level-set theory, we detail the existing methods we decided to reimplement in our study.

#### Level-set theory

In image segmentation, level-set-based methods correspond to a class of deformable models where the shape to be recovered is captured by propagating an interface represented by the zero level-set of a smooth function which is usually called the level-set function. The evolution of the interface is generally derived through a variational formulation: the segmentation problem is expressed as the minimization of an energy functional that reflects the properties of the objects to be recovered. Formally, the minimization of this functional provides the evolution of the level-set function as a time-dependent partial differential equation (PDE) that is usually solved using finite-difference methods. These numerical schemes have been developed to obtain an accurate and unique solution; they involve upwind differencing, essentially non oscillatory schemes borrowed from the numerical solutions of conservation laws and Hamilton–Jacobi equations. In this part, we thus proposed to compare several level-set implementations in order to select the one which gives the best result in terms of accuracy and time consuming.

#### Selected state-of-the-art algorithms

- Chan Vese model: separation of two regions having homogenous intensities.

This method aims at minimizing the variance inside and outside the surface during its evolution. In this model, the gradient information is dropped. Thus, the energy functional depends only on region information and a regularization term. This energy is defined as a simplification of the Mumford-Shah functional under the assumption of piecewise constant images. This method has been used for the segmentation of CTA for comparison purpose in [Hernandez and Frangi, 2007](#). The corresponding evolution equation states as:

$$\frac{\partial \phi(x)}{\partial \tau} = ((I(x) - \mu_{in})^2 - (I(x) - \mu_{out})^2) \|\nabla \phi(x)\| + \alpha_{CV} \kappa \|\nabla \phi(x)\|$$

where  $\phi$  corresponds to the evolving interface,  $\alpha_{CV}$  is an hyper-parameter whose value balanced the influence between the data attachment term and the regularization one.  $\mu_{in}$  and  $\mu_{out}$  are the mean values computed inside and outside the involving interface at each iteration and  $\kappa$  corresponds to the local curvature computed at point  $x$ .

- Gan model: optimal threshold based on maximum intensity projection images

This method exploits properties of maximum intensity project (MIP) images to derive an optimal threshold value in order to separate the vessel pixels from the rest of the image. The authors proposed to use this threshold strategy inside a classification approach in order to segment vessels. Since we decide to use deformable model, we propose to involve the corresponding feature function in a

classical level-set framework. The resulting evolution equation is composed by two terms: one region term based on the threshold value and one contour term based on a simple regularization of the interface.

The corresponding evolution equation states as:

$$\frac{\delta\phi(x)}{\delta\tau} = \text{sign}(T - I(x)) \|\nabla\phi(x)\| + \alpha_G \kappa \|\nabla\phi(x)\|$$

where  $\alpha_G$  is an hyper-parameter whose value balanced the influence between the data attachment term and the regularization one,  $T$  is the “optimal” threshold value computed from MIP images. The basic concept is the following. As compared with the original 3DRA volume, there is a larger proportion (around 20%) of vessels in its corresponding maximum intensity projection (MIP) image. The proposed method thus exploits this property to increase the accuracy of the threshold value computed from the statistical modeling with the Expectation-Maximization algorithm. Fig. 2-b shows the intensity distribution computed from the entire volume given in Fig. 2-a. From that example we can clearly see that since the amount of voxels that are responsible for the vessel is very low, the repartition of the two distributions in the image is unbalanced, making the separation of them difficult.

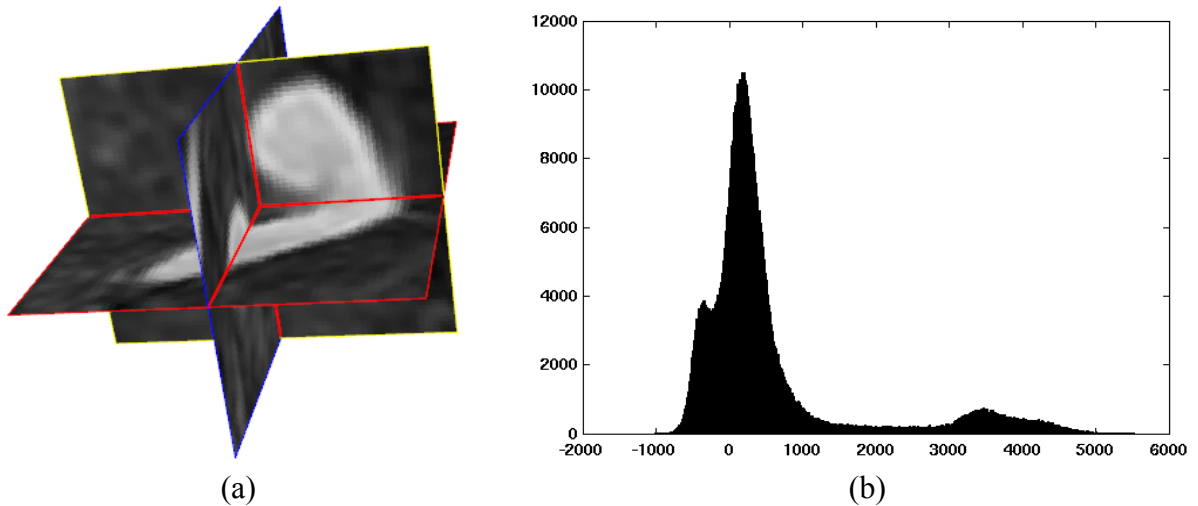


Fig. 2: Intensity profile of an 3DRA volume

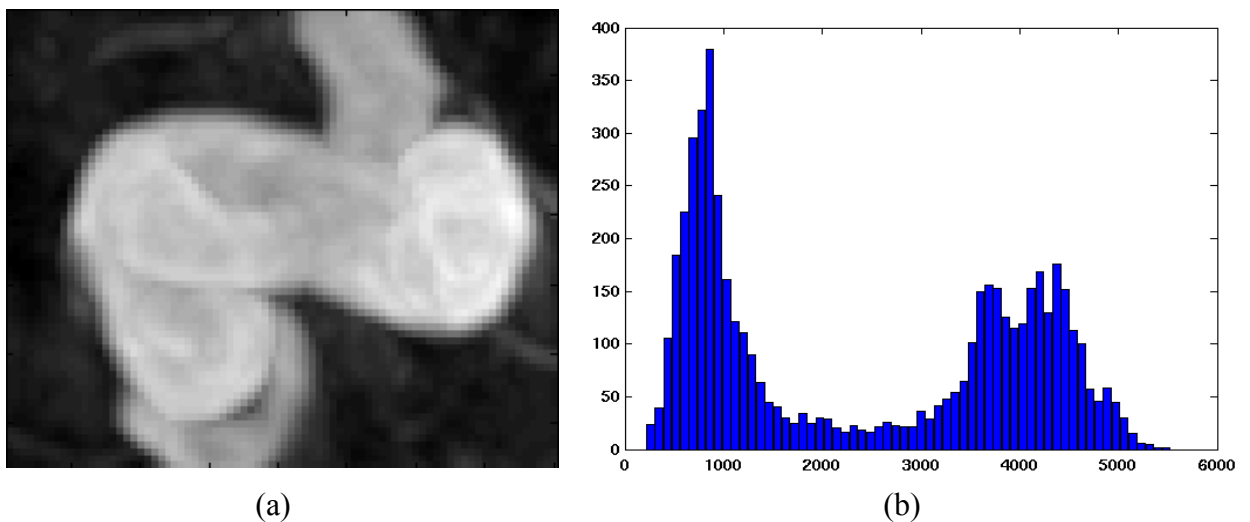


Fig. 3: Intensity profile of a MIP image created from the volume given in Fig. 1-a

In contrary, the intensity profile of the derived MIP image along the z-axis (Fig. 3-a) presents two distributions whose repartitions are more homogeneous (Fig. 3-b), making the separation of them (and so the selection of the “optimal threshold”) more accurate and robust.

- Holtzman-Gazit model: extraction of thin structures based on alignment with change of intensity

This method is adapted for the extraction of thin structures. The model is based on a weighted sum of three integral measures that account for the minimal variance within each region (Chan-Vese model), the alignment of the boundary with the change of intensity, and the weighted arc length for regularization. This method has been proposed for the segmentation of CTA in [Holtzman-Gazit et al., 2006](#). The corresponding evolution equation states as:

$$\frac{\partial \phi(x)}{\partial \tau} = \left( I_{\xi\xi}(x) - \beta((I(x) - \mu_{in})^2 - (I(x) - \mu_{out})^2) \right) \|\nabla \phi(x)\| + \gamma \operatorname{div} \left( g(x) \frac{\nabla \phi}{\|\nabla \phi(x)\|} \right) \|\nabla \phi(x)\|$$

where  $\beta$  and  $\gamma$  are two hyper-parameters.  $g(\cdot)$  is an edge function whose purpose is to enhance edges that are present in the image. In [Holtzman-Gazit et al., 2006](#), the authors proposed to use the following function:

$$g(x) = \frac{1}{1 + \left| \frac{\nabla I(x)}{\alpha} \right|^2}$$

$I_{\xi\xi}$  is an edge alignment term that tends to track edges of objects with low contrast compared to the background. Its expression states as:

$$I_{\xi\xi} = \Delta I - \operatorname{div} \left( \frac{\nabla I}{\|\nabla I\|} \right) \|\nabla I\|$$

### Initialization procedure

For all the images of the database, we perform the same simple initialization strategy: we ask a user to give one click inside the aneurysm of interest. From the selected point, we then created a sphere (with the same radius value for all the experiments equals to 5 pixels) and use it as an initial mask for the level-set models.

#### 3.2.3 Evaluation / validation

In this study, all the level-set are implemented in C++ using the sparse field implementation ([Whitaker, 1998](#)). This implementation allows efficiently dealing with the level-set evolution thanks to a narrow-band representation and an optimized distance map reinitialization performed at each iteration. For each of the five images of the database, we manually initialized the algorithm using the strategy described at the previous paragraph. We then performed the segmentation of the images using the 3 versions of level-set (Gan, Chan-Vese and Holtzman models). Fig. 4, 5a and 5b summarize the results we obtain for 3DRA images, 3DRA with dose images and CTA image respectively.

Even if the modalities are not the same, we first observed that the behaviors of the three algorithms are almost the same for 3DRA, 3DRA with dose and CTA images. Indeed, the visual quality of the result is comparable. However, it has to be notice that Gan’s model has some difficulties to segment tiny vessels, as shown for example with the CTA images given in Fig. 5b. These “comparable” results

could be explained by the fact that in our work we focus our effort on the segmentation of a small part of vascular tree centered to an aneurysm. As a consequence, we extract an ROI centered to the aneurysm and then we perform the segmentation inside the corresponding volume where the intensity distributions nicely characterize the aneurysm and the adjacent vessels. As a consequence, simple strategies based on “optimal threshold” (Gan’s model) or minimal variance within each region produce interesting results.

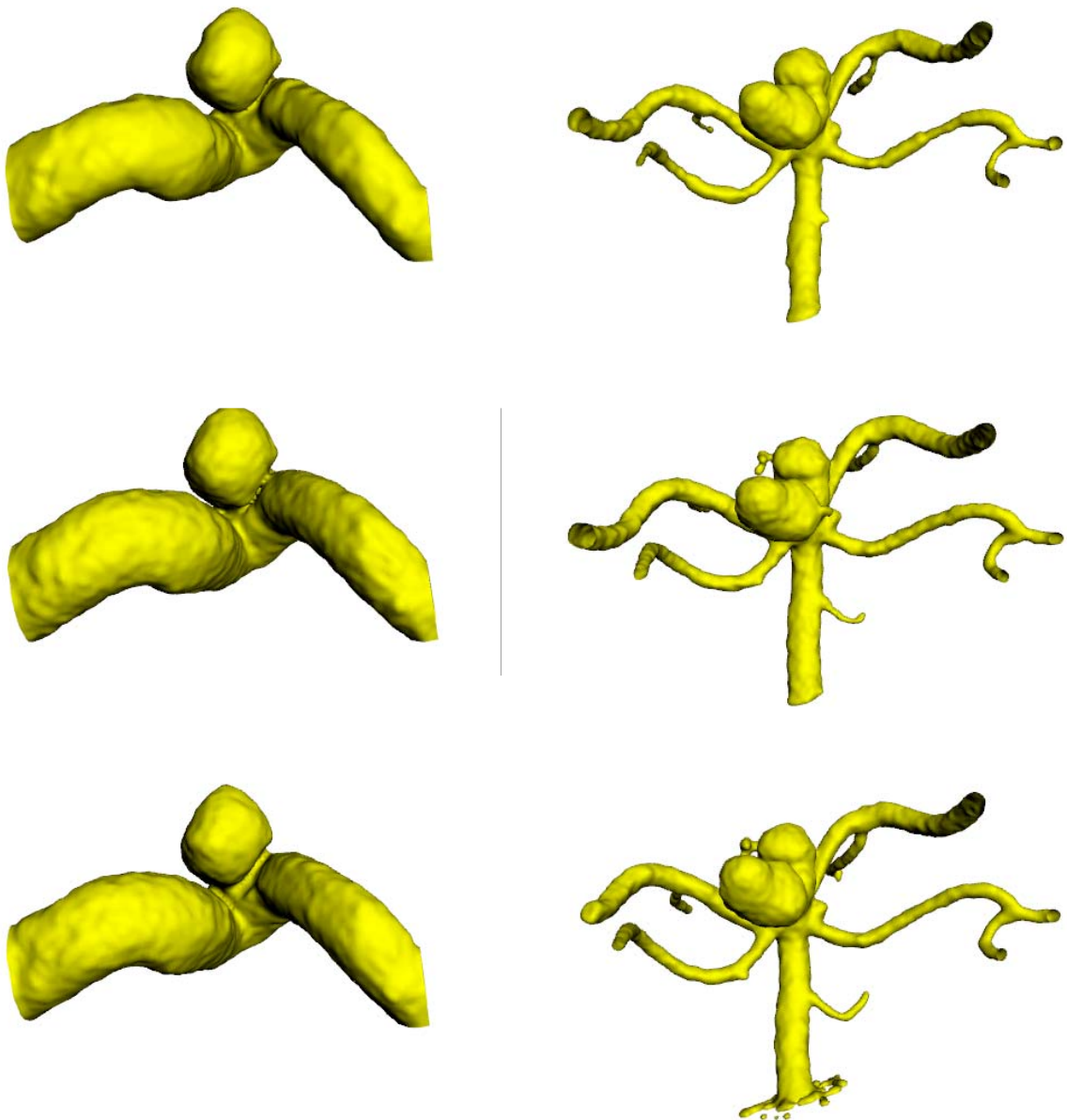


*Fig. 4: Segmentation results of two 3DRA images using state-of-the-art methods. First line: Gan model. Second line: Chan-Vese model. Third line: Holtman-Gazit model*



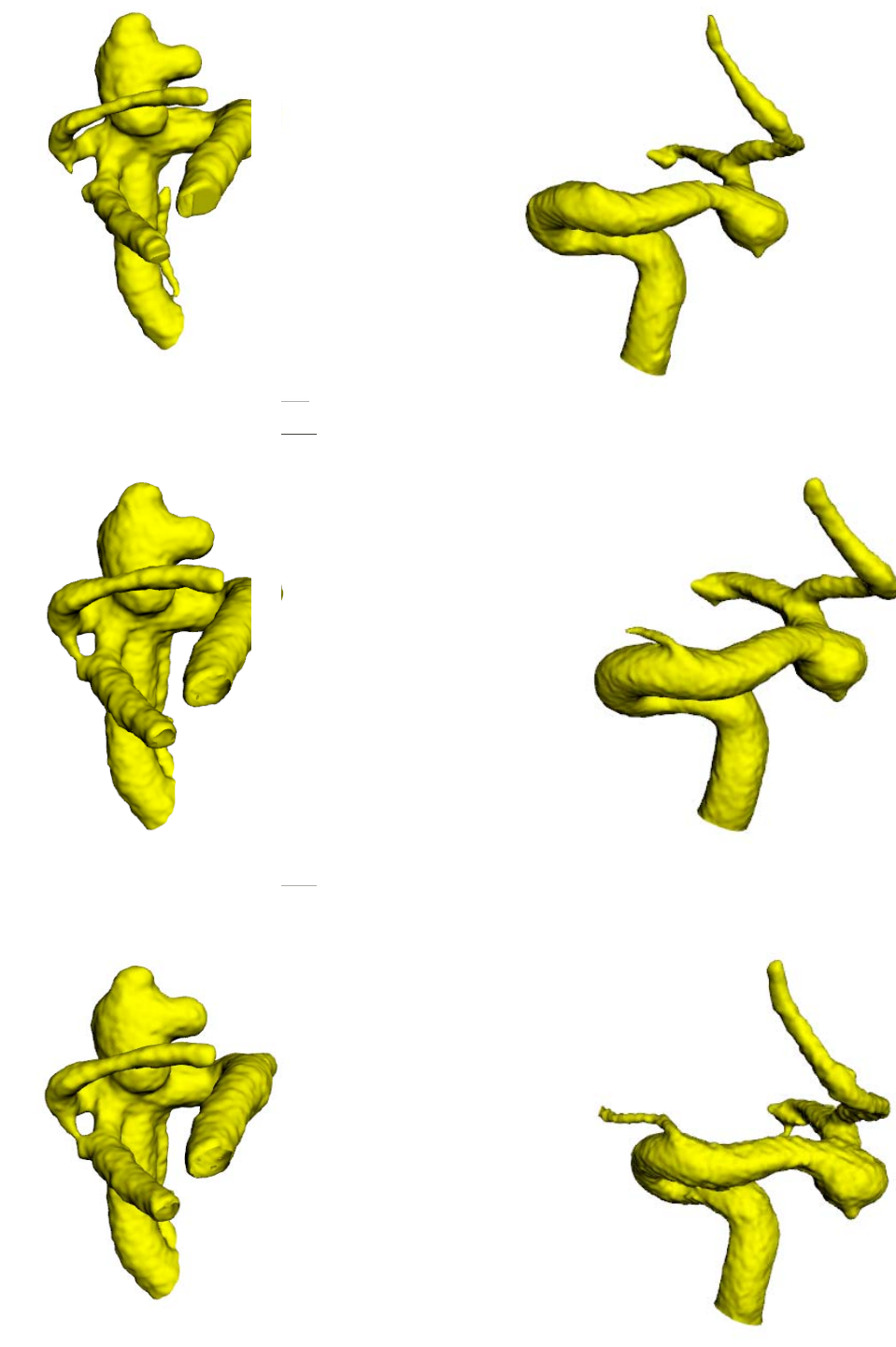


*Fig. 5 a: Segmentation results of two 3DRA with dose images using state-of-the-art methods.  
First line: Gan model. Second line: Chan-Vese model. Third line: Holtman-Grazit model*

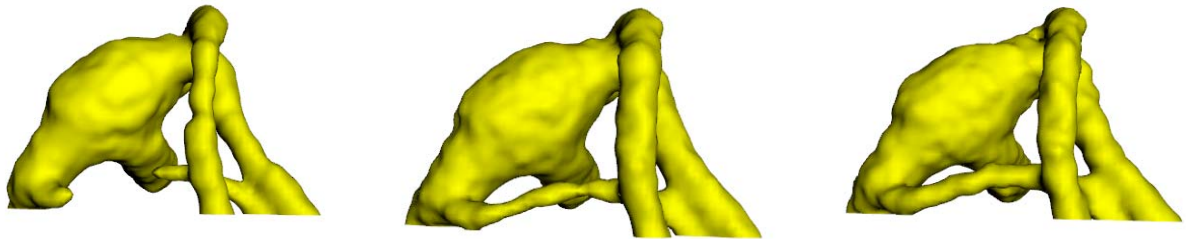


Fig. 5 b: Segmentation results of one CTA image using state-of-the-art methods. First line: Gan model. Second line: Chan-Vese model. Third line: Holtman-Grazit model

In terms of accuracy, we could notice that the three results give some slightly difference on the final results. So, in order to compare the performance of each algorithm, we have no choice but to ask an expert to manually segment images so we can compare with. We've plan to do this work the next months.

Images	Algorithms	Parameters	Number of iterations	CPU time
RA1	Gan model		240	18 s
	Chan-Vese model		349	41 s
	Holtzman model		439	65 s
RA2	Gan model		324	37 s
	Chan-Vese model		556	125 s
	Holtzman model		774	201 s
CTA2	Gan model		140	4 s
	Chan-Vese model		242	10 s
	Holtzman model		312	14 s
RAS1	Gan model		312	81 s
	Chan-Vese model		623	347 s
	Holtzman model		636	403 s
RAS2	Gan model		475	94 s
	Chan-Vese model		778	325 s
	Holtzman model		1216	1044 s

Table 1: Summary of the parameters settings used for the segmentation of the database. First column: image name. Second column: algorithms used. Third column: Parameters involved.



*Forth and fifth columns: number of iterations and CPU time needed to reach final results.*

Table 1 summarizes the hyper-parameters fixed for all the experiments along with the final number of iterations and the CPU time needed to perform the segmentation. The hyper-parameters values have been chosen in accordance with the ones given in the corresponding original papers. From these results, it can be observed that Gan's model produce the fastest results (a mean value of 27 s for 3DRA images, 87 s for 3DRA with dose images and 4 s for the CTA image). This could be easily explained by the fact that the underlying feature function is the simplest to compute and so the less time consuming at each iteration. Indeed, for both Chan-Vese and Holtzman models, one has to go through the whole volume at each iteration to update the inside and outside mean values.

Even if the obtained CPU times appear to be reasonable, we plan to put effort in the next months in significantly reducing the overall time needed to perform the segmentation of the aneurysm along with the adjacent vessels. We've already started to study some issues to tackle that problem and we will give results in the next-year deliverable.

### 3.3 Segmentation of the aneurysm structure

#### 3.3.1 Specification

Our goal in this section is to segment the aneurysm from the adjacent vessels with minimal human interaction. This problem can actually be realized as an illusory surface capturing problem by observing Fig. 6. The boundaries of the aneurysm that are not part of the blood vessel surface have to be completed naturally by illusory surface.



*Fig. 6: Left: Kanizsa triangle. Right: 2D slice of an aneurysm with and adjacent vessel. The red curves are illusory contours*

Illusory contours have been intensively studied in cognitive neuroscience, where people find that the human vision system is capable of combining nonexistent edges and making meaningful visual organization of both the real and imaginary contour segments (e.g. the Kanizsa triangle in Fig. 6). Various researchers have introduced mathematical models and techniques to mimic the human vision system in detecting and capturing ([Sarti et.al, 2000](#); [Zhu et.al, 2007](#)). Many level-set techniques have been proposed to identify missing boundaries ([Geiger et.al, 1998](#); [Jung and Shen, 2008](#)). In [Dong et.al, 2010](#), the authors proposed a nice review of level-set models applied to illusory contours detection and derived a method specifically designed for the segmentation of aneurysm. The main drawbacks of such techniques reside in the fact that the involved evolution equation are quite complex (leading to difficulties in the implementation issue and the choice of hyper-parameter values) and that they greatly depend on the algorithm initialization.

An interesting solution that is poorly influenced by the initialization has been introduced by [Sarti et. al, 2000](#). In their work, they first chose a fixation point inside the domain bounded by the ideal illusory contour, and constructed a surface on the whole domain on the basis of the point, then evolve the entire surface based on the image gradient. The Subjective Surfaces has been successfully applied in many medical applications such as membrane recovery in confocal microscopic imaging ([Zanella et. al, 2010](#)).

### 3.3.2 Strategy

From the literature, we decide to use the subjective surface framework. Indeed, this framework has already proven its ability to naturally separate objects having common boundaries with the main advantage to be simple to implement. However, we keep in mind that this method is known to be slow in 3D. In this context, our strategy is the following. Firstly, we perform the segmentation of both aneurysm and the adjacent vessel using one of the level-set framework describe in the previous section. This step is initialized by a user given one simple click inside the aneurysm. Then, from the obtained binary volume and getting used of the position of the starting point, we perform the separation of the aneurysm from the adjacent vessel using an improved version of the subjective surface.

### 3.3.3 Proposed algorithm : an improved version of subjective surface

#### Subjective surface theory

Before given the novelties we proposed in the section, we have to introduce the concept of subjective surface. This tool has been introduced (Sarti et. al., 2000) to segment objects characterized by a wide absence of information on boundaries. Such peculiarity makes the model suitable especially for this particular application. The proposed procedure requires two preliminary steps: a low level image features extraction and an initial point inside the object of interest. Since we are working on a binary volume obtained from the method described at the previous section, we use the classical edge detector  $g_s(.)$  given by:

$$g_s(x, y, z) = \frac{1}{1 + (|\nabla G_\sigma(x, y, z) * I(x, y, z)|)^2}$$

where  $G_\sigma(x, y, z)$  is a Gaussian kernel with standard deviation  $\sigma$ ,  $*$  denotes the convolution operator and  $I = I(x, y, z)$  represents the binary image obtained from Holtzman level-set strategy described in the previous section. Since we worked on a binary image, we will obtain a perfect contour of one pixel-width by setting  $\sigma = 1$ . Moreover, since the user is asked to click one point inside the aneurysm for the segmentation procedure described in the previous section, we already have the starting point needed to initialize the subjective surface procedure.

The method of Subjective Surfaces, as introduced in (Sarti et. al., 2002) consists, in the 3D case, in the volume minimization of a 3-D manifold embedded in a 4-D Riemannian space with a metric constructed on the image itself. Starting from a point inside the object to be segmented, an initial function  $\Phi_0 = \Phi_0(x, y, z)$  is then constructed, in the image domain  $\Omega$ , usually as a distance or peak function. Let us define  $\Phi = \Phi(x, y, z, \tau)$  an evolution of  $\Phi_0$ , where  $\tau$  represents a synthetic time.  $\Phi$  is evolved afterward by a mean curvature motion to minimize the volume of the hypersurface  $S$  through the following motion equation

$$\frac{\partial \Phi}{\partial \tau} = gH + (\nabla g \cdot \nabla \Phi) \quad (1)$$

with

$$H = \frac{(1 + \Phi_x^2 + \Phi_y^2)\Phi_{zz} + (1 + \Phi_x^2 + \Phi_z^2)\Phi_{yy} + (1 + \Phi_y^2 + \Phi_z^2)\Phi_{xx}}{1 + \Phi_x^2 + \Phi_y^2 + \Phi_z^2} - 2 \frac{\Phi_x \Phi_z \Phi_{xz} + \Phi_x \Phi_y \Phi_{xy} + \Phi_y \Phi_z \Phi_{yz}}{1 + \Phi_x^2 + \Phi_y^2 + \Phi_z^2}$$

Subscripted denote shorthand notations for derivatives, i.e.  $\Phi_x = \partial \Phi / \partial x$ ,  $\Phi_{xx} = \partial^2 \Phi / \partial x^2$  and  $\Phi_{xy} = \partial^2 \Phi / \partial x \partial y$ , and similarly for other spatial variables.

This model equation can then be read as in the following. The first term on the right side of (1) represents a mean curvature flow, a parabolic motion that evolves the hyper surface in normal direction with a velocity given by the mean curvature  $H$  and weighted by the edge indicator  $g$ . The second term is a pure passive advection along the velocity field – gradient of  $g$ , whose direction and strength depend on position. This term attracts the hyper surface in the direction of the image edges. Locally, different behaviours can be identified in the image regions according to one of these flows. In the homogeneous regions  $g = 1$  and gradient of  $g \rightarrow 0$ , therefore (1) reduces to the mean curvature flow: inside the objects the hyper surface levels collapse in a point and then disappear. In regions where the edge information exists,  $g \rightarrow 0$  and (1) reduces to a simple advection equation: the hyper surface levels are driven towards the edges by the field – gradient of  $g$ , their accumulation causes the increase of the spatial gradient and the hyper surface  $S$  starts to generate discontinuities. In regions with subjective contours (missing boundaries), continuation of existing edge fragments, (1) can be approximated by a geodesic flow, allowing the boundary completion with geodesics. The application of these dynamics is clear in Fig. 7, showing the effect of boundary completion in a 2D slice of real rotational angiography image of an aneurysm along with its adjacent vessel.

### 3.3.4 Originality

The subjective surface theory suffers from two main drawbacks:

- at the convergence of the hyper surface evolution, there exists no rule to fix the level at which we have to cut in order to extract the final contour. A value of level too high will imply the extraction of an under-determined contour whereas a value of level too low will imply the detection of an over-segmented contour as illustrated in Fig. 8. This level value is usually selected empirically and thus strongly influences the quality of the result. Any improvement on this particular aspect would strongly improve the subjective surface theory by making the quality of the result more robust.
- since the segmentation of a 3D object is realized by evolving a 4D surface, there is a need of a lot of iteration to reach a convergence state, making the subjective surface a time consuming algorithm. Here again, any improvement on this particular aspect would strongly improve the subjective surface theory.

We plan to take the opportunity of this project to propose a solution for the two main drawbacks of the subjective surface theory.

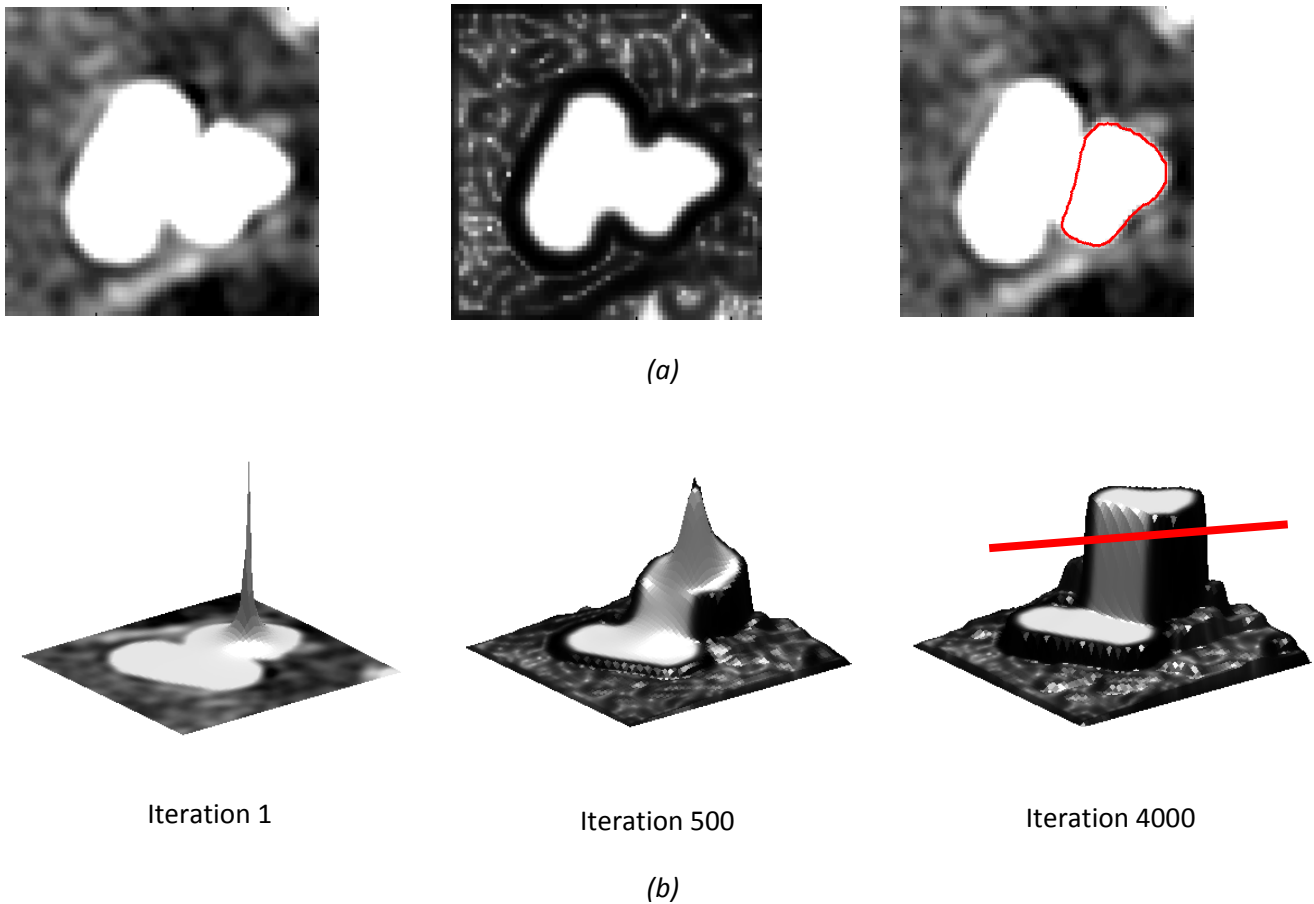


*Fig. 7: 2-D example of aneurysm segmentation from a rotational angiography image. (a, from left to right) original data, edge detector, segmented contour, in red, superimposed to original data. (b, from left to right): evolution of the initial point-of-view surface and selection of a level set, red line, for segmentation.*

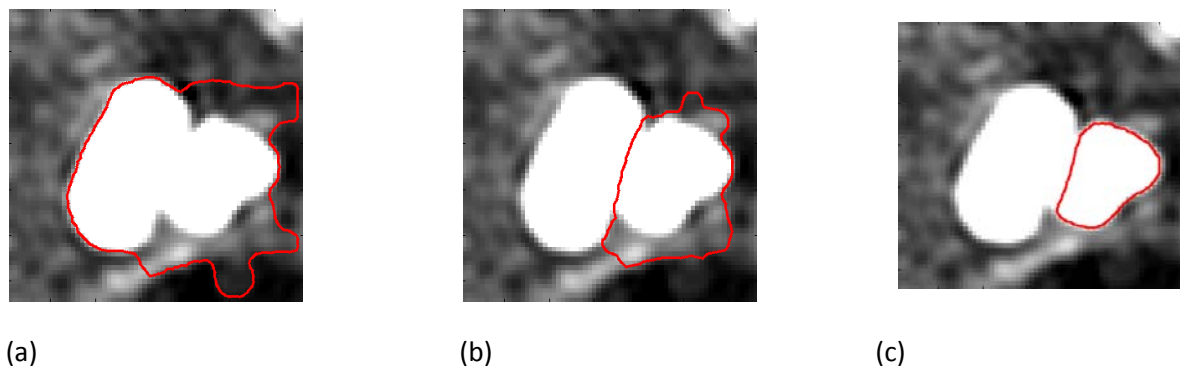


*Fig. 8. Illustration of the influence of the level value on the quality of the segmentation of an aneurysm. Segmentation result obtained for a normalized level value equals to (a) 0.3, b) 0.5 and c) 0.7.*

## Robustness from the choice of the level of the cutting plane

In order to decrease the choice of the level of the cutting plane, we take advantage of the evolution scheme of the subjective surface. Indeed, as described in paragraph 3.3.3, the subjective surface evolution is governed by two terms, a mean curvature flow and a pure passive advection term. In this part, we focus our intention on the first term, which makes the hypersurface evolve in the normal direction with a velocity given by the mean curvature  $H$  and weighted by the edge indicator  $g$ . In the particular case where  $g=1$ , this term makes the subjective surface behave as an ice melt as illustrated in Fig. 9. Indeed, it tends to smooth sharp areas of the hypersurface.

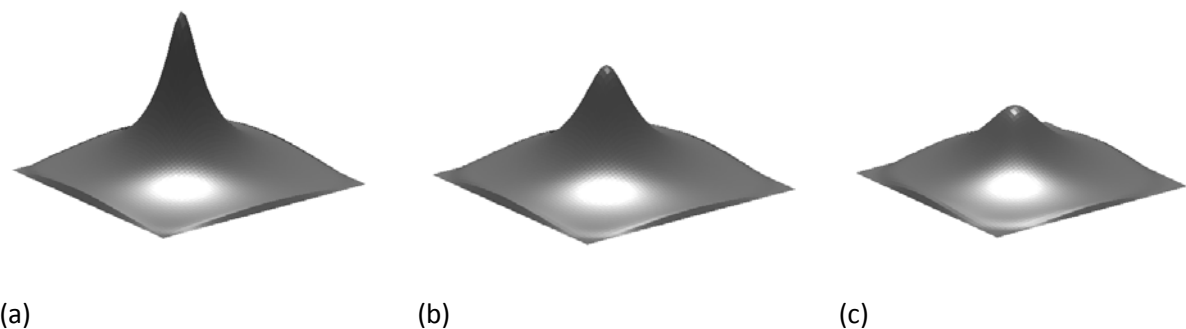


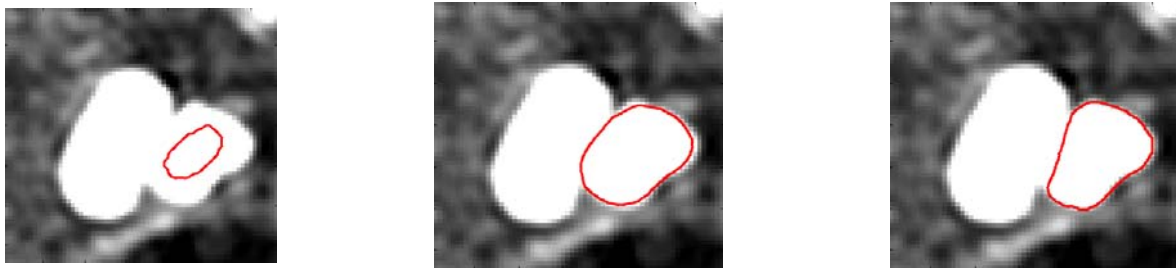
*Fig. 9. Illustration of the effect of the first term of the evolution equation on the behavior of the subjective surface. In this particular case, the subjective surface only evolves from a  $g$  function equals to 1 everywhere. (a) Initial state. b) Subjective surface after 100 iterations. c) Subjective surface after 200 iterations.*

If the initial subjective surface involves regions that are already flat, they should not be affected by this term and thus should remain almost at the same level over time. We thus propose to initialize the subjective surface by getting use of a mask ( $M$ ) inside the object of interest. From that mask, we initialize a surface using the following mathematical definition:

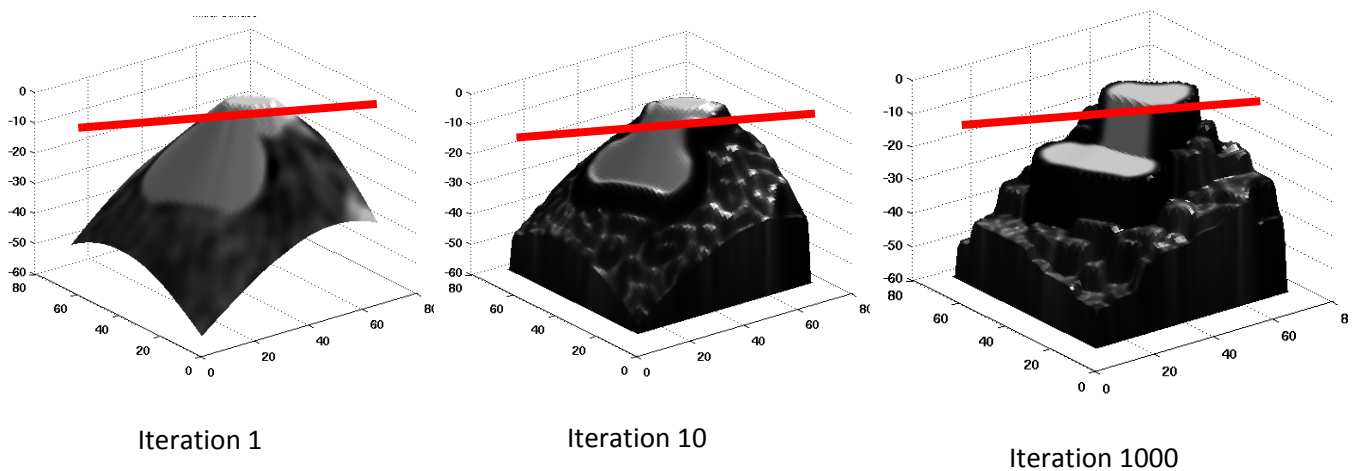
Since the mask corresponds to a flat region of the subjective surface, it should not evolve so much over time. The “optimal” level of the cutting plane should then be close to zero at the end of the segmentation process. In order to illustrate that idea, we propose in Fig. 10 to segment a 2D slice of an aneurysm from a rotational angiography imaging. The subjective surface is initialized from the mask given at the first image of Fig. 10-a. We show in Fig. 10-b the evolution of the subjective surface along with the corresponding contour extracted from a constant level equal to 5% of the initial dynamic of the hyper surface elevation (Fig. 10-a).

At that stage, we now just have to create a mask close to the aneurysm boundaries. We propose the following scheme in order to achieve that goal:

1. The user had to click on one point inside the aneurysm to initialize the level-set model presented in the previous section. From that point, we do beams tracing as illustrated in Fig. 11-b. Since we use the binary image obtained after level-set segmentation, it is simple to stop each beam at the boundary of the aneurysm or vessel interfaces.
2. From the set of beams, we compute the mean length (Me) and the corresponding standard deviation (SD). Then we keep only the beams whose length belongs to the interval  $[Me - 3SD; Me + 3SD]$ . The corresponding beams are drawn in blue in Fig 11-b.
3. From this set of selected beams, we fit a simple ellipse in 2D (Fig 11-c) or an ellipsoid in 3D (Fig. 12-a and 12-b). Note that in order to ensure that the ellipse will stay inside the aneurysm structure we subtract for each selected beam a constant distance value of 3.



(a)



(b)

*Fig. 10. Segmentation of a 2D slice of an aneurysm from a rotational angiography imaging using subjective surface theory. The red line corresponds to the level at which we extract the contour displayed on the first row.*



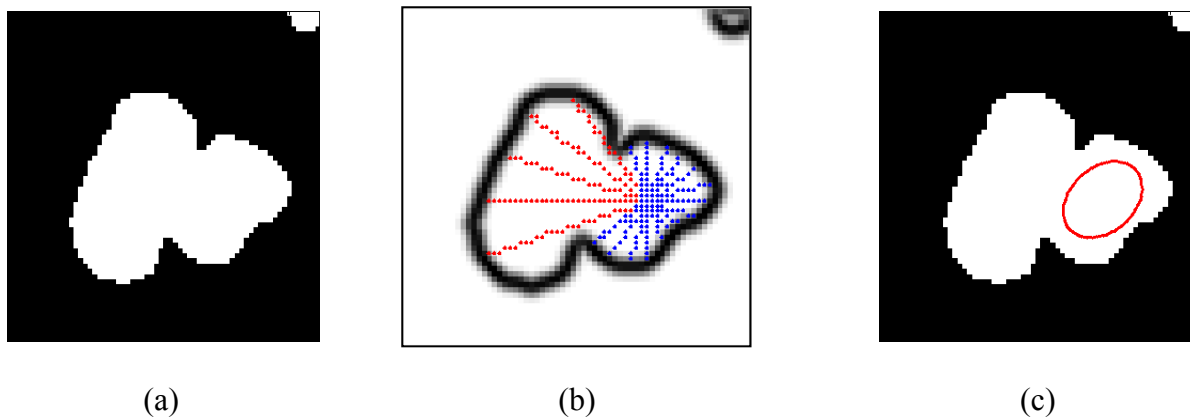


Fig. 11. 2D illustration of the creation of the initial mask inside the aneurysm

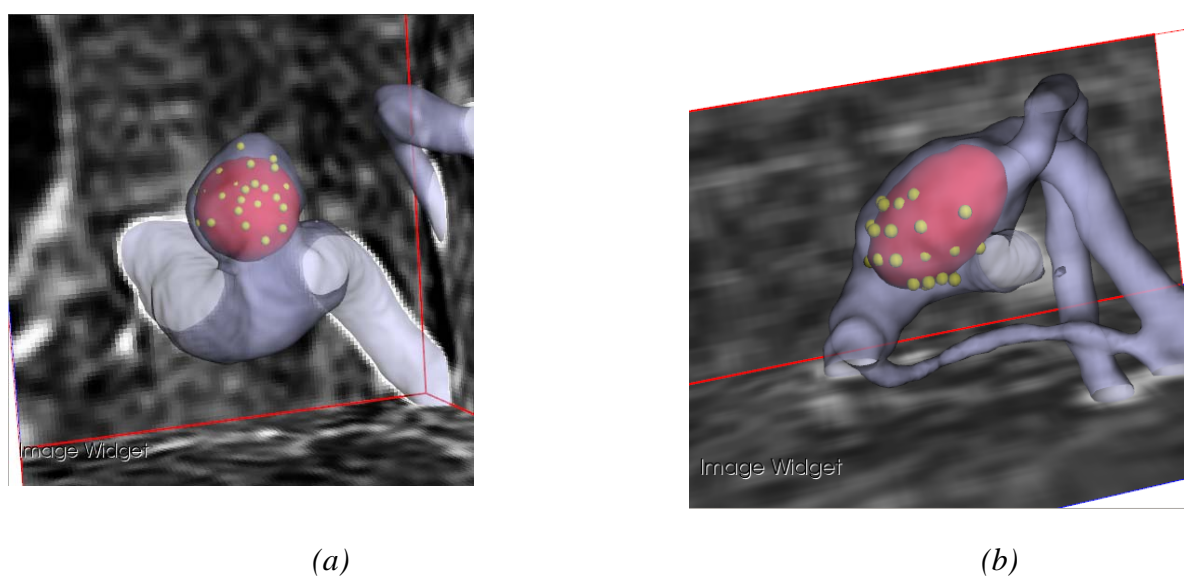
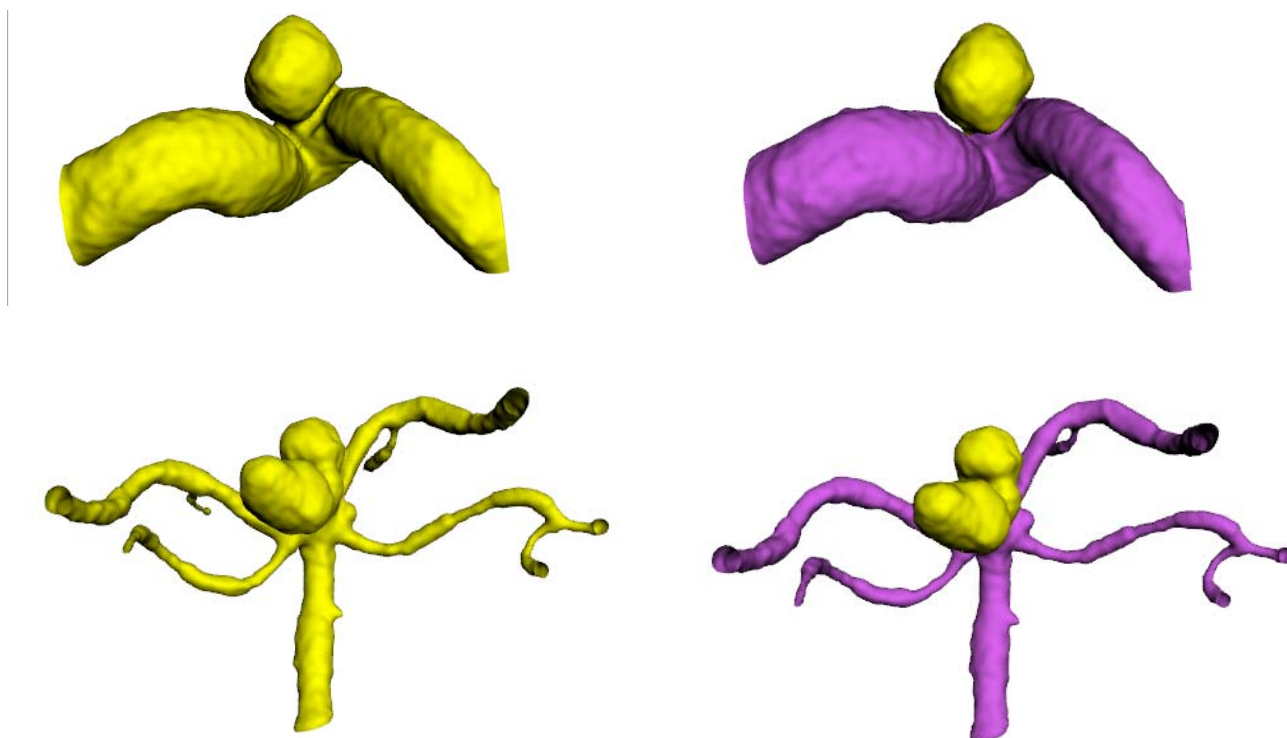


Fig. 12. Initialization procedure applied on a Rotational Angiography image (a) and a Computed Tomography Angiography image (b).

Images	Number of iterations	CPU time
RA1	1000	8s
RA2	1000	30s
CTA1	1000	6s
RAS1	1000	47s
RAS2	1000	19s

Table 2: Time spent to separate the aneurysm from the adjacent vessels. First column: image name. Second column: number of iterations. Third column CPU time needed to reach final results



*Fig. 13: Aneurysm segmentation results of two 3DRA images using a modified version of the subjective surface algorithm. First column: Vessel segmentation using Holtman-Grazit method. Second column: Aneurysm segmentation result*



*Fig. 14. Aneurysm segmentation results of a CTA image using a modified version of the subjective surface algorithm. Left image: Vessel segmentation using Holtman-Grazit method. Right image: Aneurysm segmentation result*

### 3.3.5 Evaluation / validation

The evaluation of the aneurysm separation from the adjacent vessels is very tedious. Indeed, the shared boundary is usually not well defined and could lead to subjective interpretation from experts. At the moment, the validation we made is purely visual in the sense that we verify the ability of our designed algorithm to separate the aneurysm from the rest of the vessel tree. Fig 16 gives an illustration of such result.



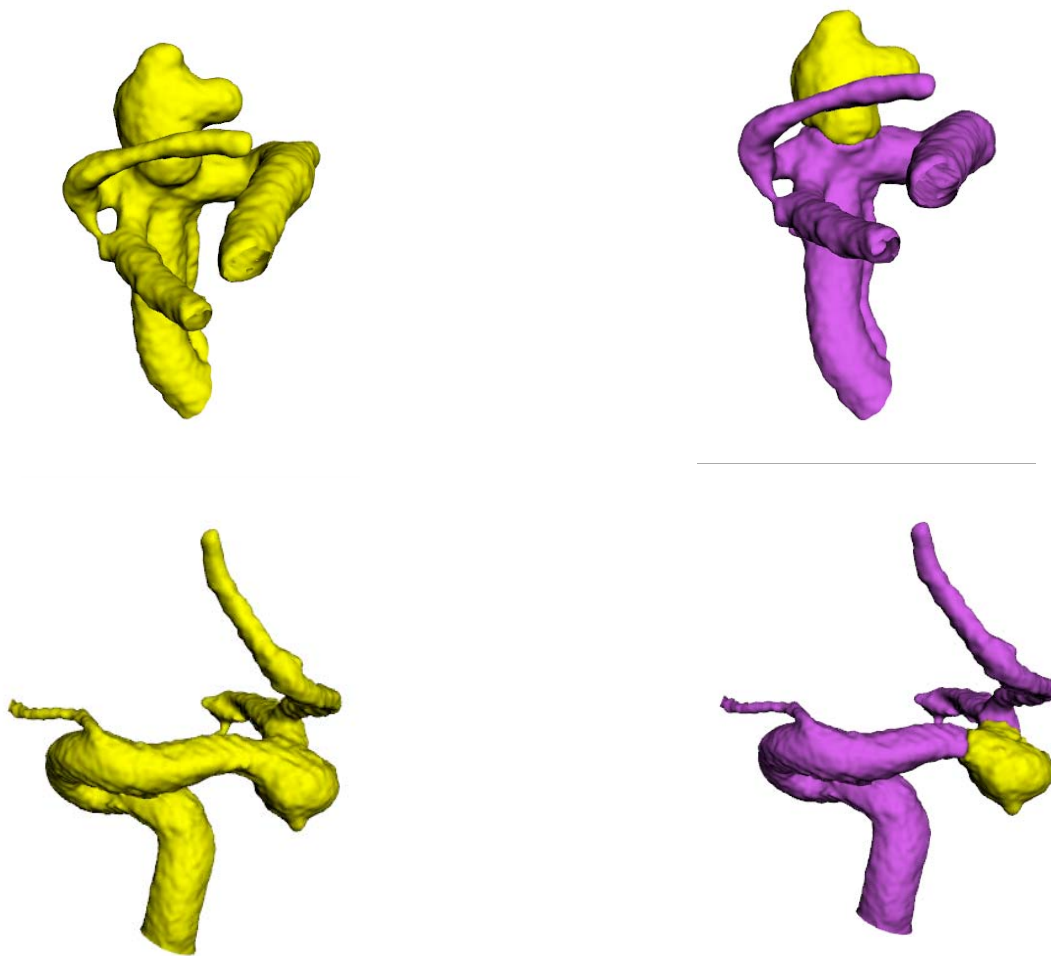


*Fig. 15. Aneurysm segmentation results of two 3DRA images with dose using a modified version of the subjective surface algorithm. First column: Vessel segmentation using Holtman-Grazit method. Second column: Aneurysm segmentation result*

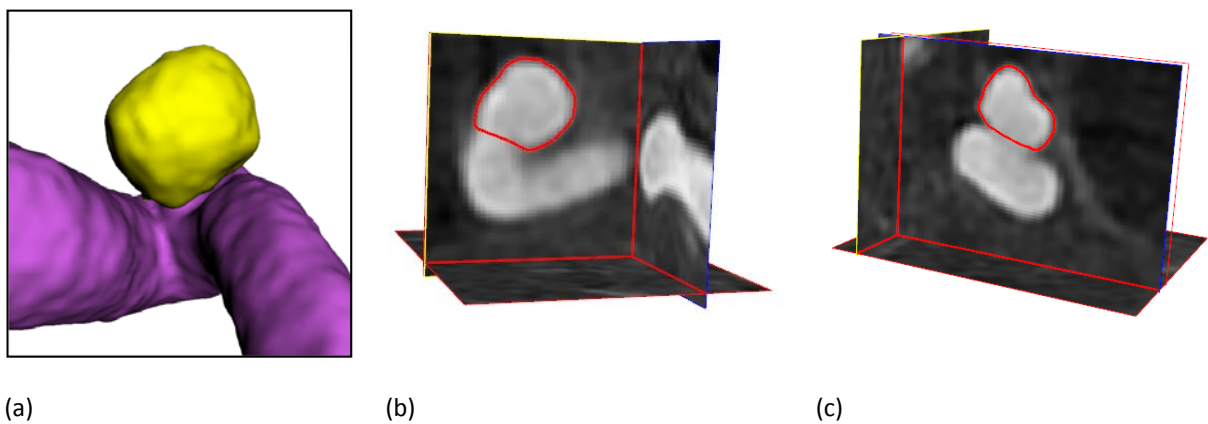


*Fig. 16. Illustration of the visualization of the 3D contour extracted from the aneurysm segmentation result.*

As for the vessel part, we plan in the next months to validate our approach by comparing our aneurysm segmentation results with the contours given by experts. Table 2 gives the number of iteration along with the corresponding CPU time needed to reach the aneurysm segmentation. From the given values, it can be seen that the actual C++ implementation needs less than 1 minute to reach the final result. Even if the obtained CPU times appear to be reasonable, we also plan to investigate times in the future in order to significantly reduce the overall time needed to perform the separation of the aneurysm with the adjacent vessels. We've already started to study some issues to tackle that problem based on GPU program.

### 3.4 Segmentation of the lumen and of the thrombus of the aneurysm

#### 3.4.1 Specification

By now there is no existing fast method that can segment aneurysm in medical images, which includes two parts, one is so-called lumen, and the other is thrombus. Segmentation of cerebral aneurysms composed of lumen and thrombus in computed tomography angiography remains a challenge for image processing community. Also, the Lattice Boltzmann method can be a good candidate for segmentation. By introducing a particular collision function based on a diffusion equation for example, the modified lattice Boltzmann equation can be a powerful tool for the segmentation of noisy and under contrasted images. Today, scientific researchers work on this direction and provide interesting results on different applications. For example, Yu Chen and Q.C. Chang applies this method for segmentation of medical images of the brain ([Chen, 2009](#), [Chang 2009](#)).

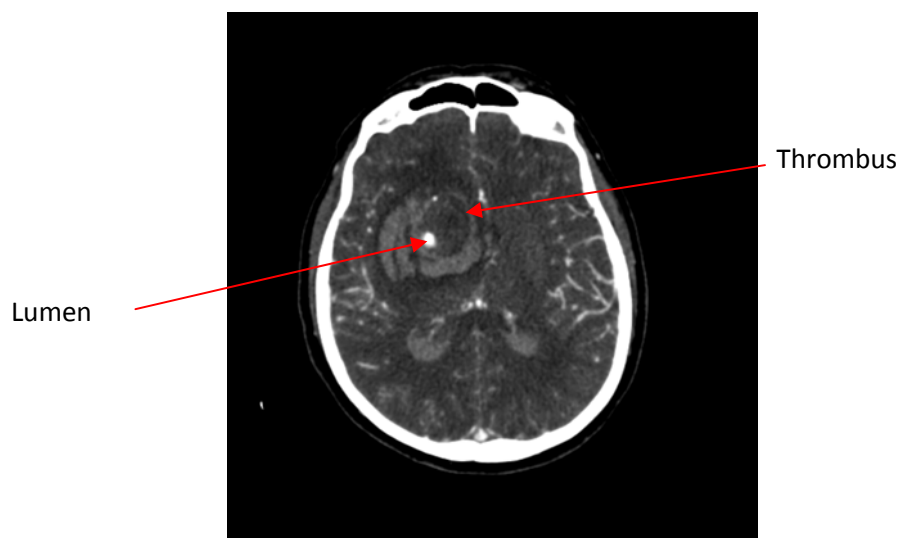


*Fig. 17 Angiographic medical image of aneurysm*

A multilevel object detection scheme based on lattice Boltzmann method (LBM) to tackle this problem is created and adapted to intracranial aneurysms. The LBM is a today usual mesoscopic mathematical tool devoted to solving macroscopic fluid dynamics problems. The idea of the LBM is to construct a simplified discrete dynamics to simulate the macroscopic model described by partial differential equations (Navier-Stokes equations in case of fluid mechanics problem). The general lattice Boltzmann modeling consist of two steps: a translation step in which particles move from node to node on a lattice and a collision step in which particles are redistributed at each node.

### 3.4.2 Strategy

We propose to deal with the segmentation problem using the LBM. The idea consists in using a multilevel object detection scheme, i.e., we segment the lumen of the cerebral aneurysm by using the LBM. After the lumen is detected, we then perform the detection of the thrombus with the aid of a different LBM configuration coupled with an expansion technique to refine the shape of the thrombus. More precisely, a LBM-based anisotropic diffusion model to segment the lumen and the thrombus (Fig.17 & Fig. 18 a) is elaborated.

Firstly, we adapt the traditional LB equation to suit the image processing process, and we add a diffusion source in the right hand side of the evolution equation in order to segment the images. After step one, we are able to get a high-contrast image of the lumen that clearly separates the lumen with other brain tissues (Fig. 18 b). Due to the blurry boundary of thrombus and other brain tissues, the lumen and the thrombus should be viewed as a whole object ([Wang, 2011](#)).

Secondly, due to the thrombus has lower contrast, we should make the parts of the aneurysm as a whole object. Therefore, we replace the gray level of lumen by the mean value of parts of thrombus (Fig. 18 c), and then apply the LBM segmentation (Fig. 18 d) with different parameters ([Wang, 2011](#)).

### 3.4.3 Algorithm

The evolution equation of the considered LBM is given by:

$$\begin{aligned}
 f_i(\vec{r} + \delta_h \vec{e}_i, t + \delta_t) = & g_i(\vec{r}) \left\{ f_i(\vec{r}, t) + \frac{1}{\tau} [f_i^{eq}(\vec{r}, t) - f_i(\vec{r}, t)] \right\} \\
 & + [1 - g_i(\vec{r})] \left\{ f_i(\vec{r} + \delta_h \vec{e}_i, t) + \frac{1}{\tau} [f_i^{eq}(\vec{r} + \delta_h \vec{e}_i, t) - f_i(\vec{r} + \delta_h \vec{e}_i, t)] \right\} \\
 & + a\delta_t [\rho(\vec{r}) - T]
 \end{aligned}$$

$f_i(\vec{r}, t)$  is the density distribution function at node  $\vec{r}$  at time  $t$ .  $f_i(\vec{r} + \delta_h \vec{e}_i, t + \delta_t)$  is the density distribution function at node  $\vec{r} + \delta_h \vec{e}_i$ , at time  $t + \delta_t$ , with  $\delta_h$  designating lattice spacing and  $\delta_t$  time step.

The lumen and thrombus segmentation scheme is based on the following mechanism. When a particle moves to neighboring nodes, it passes through a so-called medium membrane with a probability  $g_i$  and bounces back with a probability  $(1 - g_i)$ . The state of the node at the next time is equal to the sum of the number of particles rebounded back from the membrane and the number of neighboring particles traveling through the membrane.

The right hand side of the evolution equation represents the collision term and the quantity  $\tau$  is the single relaxation time, which controls the rate of approaching to equilibrium. The last term is the diffusion source with the threshold  $T$ . The equilibrium distribution functions  $f_i^{eq}(\vec{r}, t)$  depend only on

local density and velocity. The total density per node  $\rho$ , and the macroscopic flow velocity,  $\vec{u} = (u_x, u_y)$ , are defined in terms of the particle distribution functions by:

$$\sum_{i=0}^8 f_i = \sum_{i=0}^8 f_i^{eq} = \rho, \quad \sum_{i=1}^8 f_i \vec{e}_i = \sum_{i=1}^8 f_i^{eq} \vec{e}_i = \vec{u}$$

### 3.4.4 Originality

Since, thrombus is a diffusive object whose boundary is very difficult to define. After the last step, we can only get parts of the boundary. To deal with this problem, we place a disc at each pixel of the image, and expand the disc till it covers less than 94.6% of the aneurysm. Form all of the discs, we choose the biggest one and make this disc visible, as statistically it is most similar with the aneurysm (Fig. 18 e).

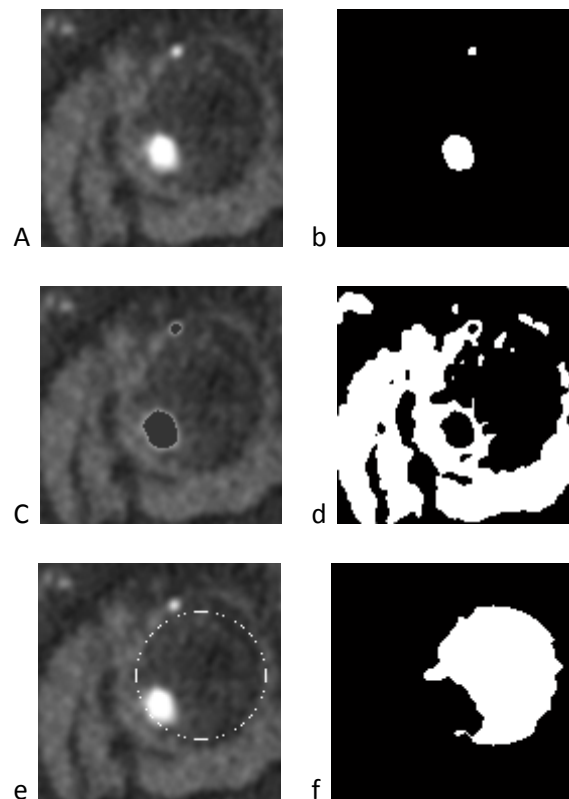


*Fig. 18. Segmentation of the lumen (b) and of the thrombus (f) of the image (a)*

With Boolean operation, we can get lumen and thrombus separately. The 2D results show that with the proposed method both lumen and thrombus can be well segmented (Fig. 18 b & f), demonstrating the promising potentiality of this LBM-based multilevel detection approach for clinical applications. The challenge now is to adapt and apply this new method to the 3D and 4D cases.

### 3.4.5 Validation

The results of segmentation are today evaluated qualitatively by the neuroradiologists of CHUV Lausanne and HCL Lyon.

## 4 Conclusion

---

### 4.1 Conclusion on the segmentation of both aneurysm and adjacent vessel part

We have first defined a strategy to perform the segmentation of both the aneurysm and the adjacent vessels. Indeed, a user is asked to click on one point inside the aneurysm. This point is then used both as an initialization for the segmentation process and as a prior information for the separation of the aneurysm from the adjacent vessels.

From the state-of-the-art in the domain, we decide to focus our interest on region-based geometric deformable models and more particularly on level-set. In this context, we study and compare the behaviour of three models (Chan-Vese, Gan and Holtzman models) involving features computed directly from the image itself and without any learning stage strategy. We observed that the three models give almost the same results. The small difference resides in the ability of the models to segment very thin structures. In this context, Holtzman model appears to give best results but with the main drawback of being time consuming

### 4.2 Conclusion on the segmentation of the aneurysm alone

We have implemented a solution based on subjective surface since this tool has already proven its ability to naturally separate objects having shared boundaries. We show that thanks to simple strategies, this algorithm provides robust results in the separation of the aneurysm from the adjacent vessel. The main drawback of this model is the computational time.

### 4.3 Conclusion on the segmentation of both the lumen and the thrombus of the aneurysm

The segmentation of lumen and thrombus has been computed by the lattice Boltzmann method for a 2D case: a giant cerebral aneurysm. The result is relevant in the sense that we are able to propose an automatic segmentation of the thrombus by taking as a prior information the geometry of the structures.

### 4.4 Work in progress

This first-year project gave us the opportunity to define a complete strategy for the segmentation of aneurysm, adjacent vessel and thrombus regions. For the aneurysm and adjacent vessels segmentation, we program and compare three methods from the literature. Since these models give almost same results, we decide to precisely quantify the accuracy of each method. We thus plan to ask an expert to manually segment each image of the database so we will have a reference to compare with. We are aware that this work is long and tedious, so we decide to ask for the manual segmentation each time a new image is acquired from the CHU of Montpellier.

Since the separation of the aneurysm to the adjacent vessels appears to give satisfactory results, we decide to concentrate our effort for the next year on the following three points:

- Accurate segmentation of the different structures. For that aspect, as already mentioned above, we plan to build a database of references so we can efficiently evaluate the degree of accuracy of the proposed method. From the state-of-the-art study we made, we think that there exists still research to do to improve the accuracy of the extraction of thin structures. We thus plan to propose for the next year an original approach to provide accurate segmentation of thin vessels.
- Significant decrease of the actual time needed to perform the segmentation tasks. Indeed, from the results we obtained, we can conclude that the segmentation of both aneurysm and adjacent

vessel takes in average 47s with an optimized version of level-set in C++. So we will strongly put effort in the next year to significantly decrease the computational time needed in our environment. In this context, we plan to work on two complementary aspects. First, we have the idea to propose a modified version of the current level-set evolution in order to efficiently take into account the particularity of vessel segmentation. We then plan to investigate time to propose an efficient GPU implementation of both level-set and subjective surface.

- The challenges concerning the segmentation of the thrombus by the Lattice Boltzmann methods applied to image processing, will consist in the design of a generalized formulation of the diffusion function in the collision operator. By the way, the implementation of 3D models will be performed. The 4D case needs to find new concepts applied to dynamic data provided by the medical imaging modalities (MRI 3T...).

## 5 References

Aubert, G., Barlaud, M., Faugeras, O., Jehan-Besson, S., 2003. Image segmentation using active contours: calculus of variations or shape gradients. *SIAM J. Appl. Math.* 63 (6), 2128–2154.

Caselles, V., Kimmel, R., Sapiro, G., 1997. Geodesic active contours. *Int. J. Comput. Vision* 22 (1), 61–79.

Chan, T., Vese, L., 2001. Active contours without edges. *IEEE Transactions on Image Processing*. 10, 266– 277.

Chang and, Q.C. Yang, T, A Lattice Boltzmann Method for Image Denoising, 2009, *IEEE Trans. On Image Processing*, Vol. 18, pp. 2797-2802.

Chen, Y., Lattice Boltzmann Method based Medical Image Segmentation, 2009, *IEEE Image and Signal Processing CISP'09*, 978-1-4244-4129-7.

Chung, A.C.S., Noble, J.A., Summers, P., 2004. Vascular segmentation of phase contrast magnetic resonance angiograms based on statistical mixture modeling and local phase coherence. *IEEE Trans. Med. Imaging* 23 (12), 1490–1507.

Dong, B., Chien, A., Mao, Y., Ye, J., Osher, S., 2010. Level set based brain aneurysm capturing in 3D. *Inverse Problems and Imaging (special issue in medical image analysis)*, 4(2), 241–255

Fridman, Y., Pizer, S.M., Aylward, S., Bullitt, E., 2004. Extracting branching tubular object geometry via cores. *Med. Image Anal.* 8 (3), 176–196.

Gan, R., Wong, W.C.K., Chung, A.C.S., 2005. Statistical cerebrovascular segmentation in three-dimensional rotational angiography based on maximum intensity projections. *Med. Phys.* 32 (9), 3017–3028.

Geiger, D., Pao, H. K., Rubin, N., 1998. Salient and Multiple illusory surfaces, *IEEE Computer Society Conference on Computer Vision and Pattern Recognition*, San Barbara, CA.

Hernandez, M., Frangi, A.F., 2004. Geodesic active regions using nonparametric statistical regional description and their application to aneurysm segmentation from CTA. *Medical Imaging and Augmented Reality (MIAR 2004)*. In: *Lecture Notes in Computer Science (LNCS)*, vol. 3150. Springer-Verlag, Berlin, Germany, pp. 94–102.



- Hernandez, M., Frangi, A.F., 2007. Non-parametric geodesic active regions: Method and evaluation for cerebral aneurysms segmentation in 3DRA and CTA. *Medical Image Analysis*. 11, 224-241.
- Holtzman-Gazit, M., Kimmel, R., Peled, N., Goldsher, D., 2006. Segmentation of thin structures in volumetric medical images. *IEEE Trans. Med. Imaging* 15 (2), 354–363.
- Jung, Y. M. and Shen, J., 2008. First-order modeling and stability analysis of illusory contour. *Journal of Visual Communication and Image Representation* archive, 19(1), pp. 42–55.
- Manniesing, R., Velthuis, B.K., van Leeuwen, M.S., van der Schaaf, I.C., van Laar, P.J., Niessen, W.J., 2006. Level set based cerebral vasculature segmentation and diameter quantification in CT angiography. *Med. Image Anal.* 10, 200–214.
- Osher, S., Sethian, J.A., 1988. Fronts propagating with curvaturedependent speed: Algorithms based on Hamilton–Jacobi formulations. *J. Comput. Phys.* 79, 12–49.
- Otsu, N., 1979. A Threshold Selection Method from Gray-Level Histograms. *IEEE Transactions on Systems, Man, and Cybernetics*. 9, 62-66.
- Paragios, N., 2000. Geodesic active regions and level set methods: contributions and applications in artificial vision. Ph.D. thesis, University of Nice Sophia-Antipolis, France.
- Pichon, E., Tannenbaum, A., Kikinis, R., 2004. A statistically based flow for image segmentation. *Med. Image Anal.* 8, 267–274.
- Sarti, A., Malladi, R., Sethian, J. A., 2000. Subjective Surfaces: A Method for Completing Missing Boundaries. *Proceedings of the National Academy of Sciences of the United States of America*. 12, 6258-6263.
- Sarti, A., Malladi, R., Sethian, J.A., 2002. Subjective Surfaces: A Geometric Model for Boundary Completion. *International Journal of Computer Vision*. 46, 201-221.
- Van Bommel, C.M., Spreeuwiers, L.J., Viergever, M.A., Niessen, W.J., 2003. Level-set-based artery-vein separation in blood pool agent CE-MR angiograms. *IEEE Trans. Med. Imaging* 22 (10), 1224–1234.
- Volkau, I., Weili, Z., Baimouratov, R., Aziz, A., Nowinski, W.L., 2005. Geometric modeling of the human normal cerebral arterial system. *IEEE Trans. Med. Imaging* 24 (4), 529–539.
- Wang, Y., Courbebaisse, G., Zhu, Y. M., Segmentation of Giant Cerebral Aneurysm Using a Multilevel Object Detection Scheme Based on Lattice Boltzmann Method, 2011, *IEEE International Conference on Signal Processing, Communications and Computing*, vol. 3799, XI'AN, IEEE, September.
- Wilson, D.L., Noble, J.A., 1999. An adaptive segmentation algorithm for time-of-flight MRA data. *IEEE Trans. Med. Imaging* 18 (10), 938–945.
- Whitaker, R., 1998. A level-set approach to 3D reconstruction from range data. *International Journal of Computer Vision*. 29, 203–231

Yezzi, A., Tsai, A., Willsky, A., 1999. A statistical approach to snakes for bimodal and trimodal imagery. In: Proceedings of the Seventh IEEE International Conference on Computer Vision, vol. 2, 1999, pp. 898–903.

Zanella, C., Campana, M., Rizzi, B., Melani, C., Sanguinetti, G., Bourguine, P., Mikula, K., Peyrieras, N., Sarti, A., 2010. Cells Segmentation From 3-D Confocal Images of Early Zebrafish Embryogenesis. IEEE Trans. Image Process. 19 (3), 770–781.

Zhu, W. and Chan, T. F., 2007. A Variational Model for Capturing Illusory Contours Using Curvature. J. Math. Imaging and Vision, 27 (1), pp. 29–40.

Zhu, S.C., Yuille, A., 1996. Region competition: unifying snakes, region growing, and Bayes/MDL for multiband image segmentation. IEEE Trans. Pattern Anal. Mach. Intell. 18 (9), 884–900.